

A transonic small-disturbance model for the propagation of weak shock waves in heterogeneous gases

By THOMAS E. GIDDINGS¹†, ZVI RUSAK²
AND JACOB FISH³

¹Metron Inc., 11911 Freedom Dr., Suite 800, Reston, VA 20190-5602, USA

²Department of Mechanical Engineering, Aeronautical Engineering, and Mechanics,
Rensselaer Polytechnic Institute, 110 8th Street, Troy, NY 12180-3590, USA

³Department of Civil Engineering, Rensselaer Polytechnic Institute, 110 8th Street, Troy,
NY 12180-3590, USA

(Received 10 January 2000 and in revised form 9 September 2000)

The interaction of weak shock waves with small heterogeneities in gaseous media is studied. It is first shown that various linear theories proposed for this problem lead to pathological breakdowns or singularities in the solution near the wavefront and necessarily fail to describe this interaction. Then, a nonlinear small-disturbance model is developed. The nonlinear theory is uniformly valid and accounts for the competition between the near-sonic speed of the wavefront and the small variations of vorticity and sound speed in the heterogeneous media. This model is an extension of the transonic small-disturbance problem, with additional terms accounting for slight variations in the media. The model is used to analyse the propagation of the sonic-boom shock wave through the turbulent atmospheric boundary layer. It is found that, in this instance, the nonlinear model accounts for the observed behaviour. Various deterministic examples of interaction phenomena demonstrate good agreement with available experimental data and explain the main observed phenomena in Crow (1969).

1. Introduction

Many problems involving the propagation of weak shock waves, or acoustic waves in general, must account for slight heterogeneities in the media. One of the most notable examples is the sonic-boom problem, which will be used to frame the present discussion, though the theory presented herein applies to the general situation involving acoustic waves in heterogeneous media. It is well known that a supersonic aircraft produces shock waves, which often extend to the ground where they are in turn reflected. A schematic of the basic wave system produced by such an aircraft is depicted in figure 1, where only the leading-edge and trailing-edge shock waves and their reflected counterparts are sketched.

In the immediate vicinity of the aircraft the disturbance pattern is a complicated system of shocks and rarefaction waves, but far from the aircraft the effects of nonlinear steepening simplify the pressure signature. At ground level the pressure signature consists, roughly, of a smooth expansion situated between two weak shock waves as depicted in figure 2. An analytical study of such phenomena was provided by

† Contracted to the Naval Research Laboratory, Code 7130, Washington DC, 20375-5320 USA.

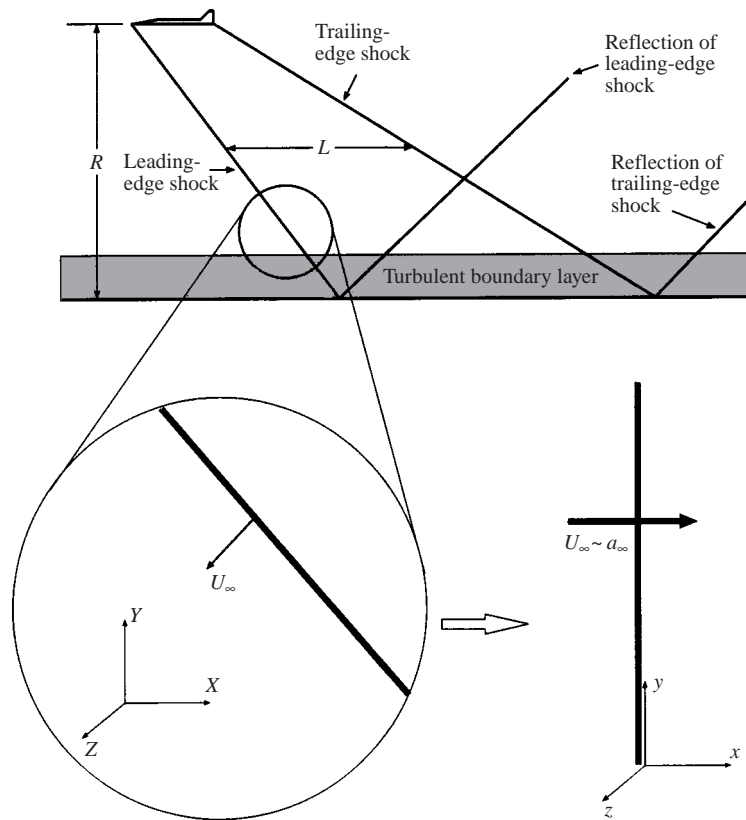


FIGURE 1. Schematic of sonic boom wave system.

Whitham (1952, 1956), who described the universal *N-wave* shape and also provided estimates for the distance between the leading-edge and trailing-edge shock waves, L , and the strength of the shock wave in terms of the *overpressure*, Δp . These estimates presume that the atmospheric properties ahead of the leading-edge shock are uniform, with constant pressure and temperature, p_∞ and T_∞ . This homogeneous state will be referred to as the *nominal free stream*. Likewise, the *nominal N-wave* indicates the pressure signature under the same assumptions.

It is noted that the nominal pressure jump across the shocks, Δp , at ground level decreases with cruising altitude, R . The resulting shock waves are very weak in the sense that Δp is very small relative to the nominal free-stream pressure, p_∞ (the overpressure, Δp , commonly varies between 1 and 3 p.s.f.). Waves that are weak in this sense may be significant in other respects, however. For example, very small pressure waves within a certain frequency range manifest themselves as audible sound. A weak shock wave is also an example of such a pressure wave and is experienced as a sudden, loud bang. The sound produced by a supersonic aircraft is called a *sonic boom* and is of great practical concern for aerodynamicists since people tend to find loud, startling noises objectionable.

The assumption of a homogeneous atmosphere is clearly an idealization, and experimental measurements show that the predicted *N-wave* becomes quite distorted when it interacts with heterogeneities in the atmosphere (cf. Garrick 1968; Garrick & Maglieri 1968; Hubbard *et al.* 1964; Kane 1967; Kane & Palmer 1964). The

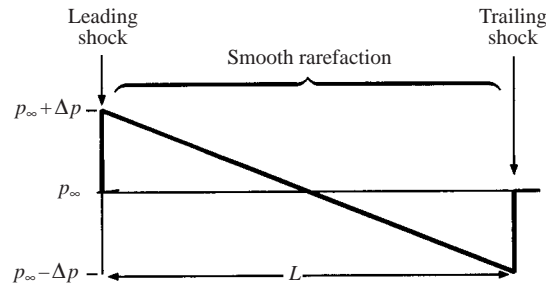


FIGURE 2. Pressure signature of nominal N-wave.

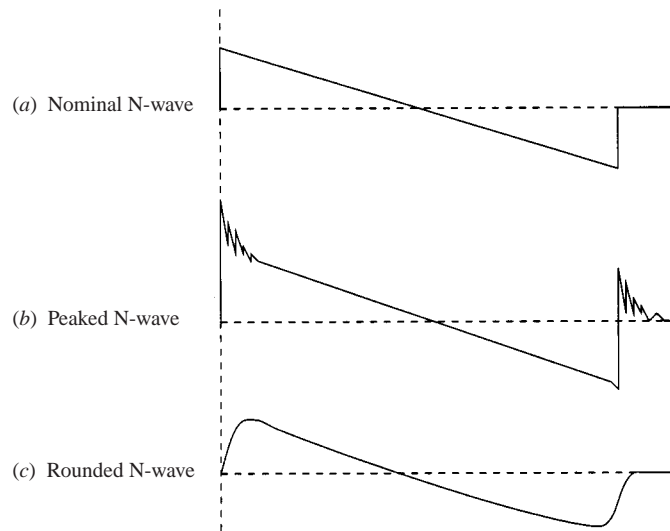


FIGURE 3. Schematic of distorted pressure profiles.

extensive direct numerical simulations by Lee, Lele & Moin (1993) also display similar behaviour. In particular, when a sonic-boom wave system encounters regions of significant atmospheric turbulence the predicted N-wave pattern may be amplified or attenuated. When the interaction results in an amplification of the shock strength, an otherwise objectionable sonic boom may become intolerably loud. The interactions which produce such amplifications have been studied for several decades and the obvious aim is to limit the noise levels or, at least, to provide reasonably accurate predictions for them.

It is generally accepted that the interaction of the shock waves with relatively small-scale fluctuations (such as atmospheric turbulence and wind gusts) produces the most pronounced and unpredictable distortions to the nominal N-wave pattern. Referring to figure 3, we may loosely classify the deviations from the nominal N-wave shape as either 'peaked' or 'rounded'. The peaked profile exhibits markedly amplified shock waves with small-scale pressure spikes immediately behind the shock front, while the rounded profile displays a smooth transition through the sonic point which is usually accompanied by an attenuated pressure rise (see review articles by Pierce & Maglieri 1972, and Plotkin 1989).

In a landmark paper, Crow (1969) examined the interaction of weak shock waves and turbulent fluctuations within the context of the sonic-boom problem. The paper

provides a detailed overview of the problem and lists several attributes of experimentally measured pressure signatures. Here we may classify the main observed characteristics, adapted from Crow (1969) and reflecting subsequent investigations, as follows:

1. The small-scale perturbations to the nominal N-wave profile are random, they fluctuate rapidly, and they may be of either sign, irrespective of the mean wind speed or the mean thermal gradient.

2. The shock wave thickness may have a length scale several orders of magnitude greater than what can be attributed to the diffusive effects of viscosity and heat conduction.

3. The amplification of the shock waves may result in an overpressure, Δp , several times greater than the nominal pressure jump.

4. The length scale of the spikes behind the incident shock increases with the distance from the wavefront. The spikes are always very small relative to the scale of the N-wave itself (L) and considerably smaller than the energy-bearing, turbulent eddies. Also, the magnitude of the pressure spikes decays rapidly behind the shock wave.

5. The perturbations to the leading-edge and trailing-edge shocks of the same wave system, incident or reflected, are nearly identical. That is, not only are the distortions either both peaked or both rounded, but also the profiles match.

6. The perturbations to the incident and reflected waves, measured at the same position, are often found to be very different.

These observations guide the present study and, using the nonlinear theory developed herein, we provide insight into each of them. The first observation is consistent with the random nature of turbulent fluctuations. The scale of turbulent eddies is such that the wave system encounters many different coherent turbulent structures in a short time and, therefore, the distortions should vary rapidly and randomly. That large-scale thermal gradients do not appear to have a pronounced effect would seem to indicate that the shock waves interact more strongly with smaller-scale fluctuations. Also, fluctuations in the mean wind speed, which are generally much stronger than the turbulent velocity fluctuations, apparently fail to induce a significant interaction. This suggests that the transverse length scales of the fluctuations influence the strength of the interaction.

According to the second observation, the length scale of the shock wave may be several orders of magnitude greater than that of a shock wave propagating in a uniform medium (about $1\ \mu\text{m}$). The problem of *shock thickening* and anomalous *rise times* (a somewhat ambiguous measure of the distance to the peak pressure) has been studied by Pierce (1970, 1971), George & Plotkin (1971), Plotkin & George (1972), Ffowcs Williams & Howe (1973), Hodgson & Johannesen (1971), Reed (1977), Bass, Ezell & Raspet (1983) and Bass *et al.* (1987), among others. In the present investigation we introduce an alternative explanation for shock thickening, in the light of a new model, which is also supported by numerical calculations.

The third observation indicates that the pressure perturbations to the nominal N-wave are of the same order of magnitude as the nominal pressure jump in the vicinity of the shock waves. One must keep in mind, however, that the overpressures, Δp , of the nominal shock waves are themselves very small perturbations to a nominally uniform free-stream pressure, p_∞ . In fact, we have two competing weak, but finite, quantities: the strength of the shock wave and the strength of the free-stream fluctuations.

According to the fourth observation, the length scales of the pressure spikes are much smaller than the length scales of the energy-bearing eddies. This observation

admits at least two explanations: (i) the energy-bearing eddies may not be responsible for inducing the interaction; or, (ii) the acoustic response to the interaction of the shock wave with these eddies has a compressed length scale. As it turns out, the acoustic waves scattered forward, towards the wavefront, are highly compressed because their progress is impeded by the oncoming flow, which is nearly sonic relative to the wavefront.

The fifth observation intimates that the characteristic time scale of the turbulent fluctuations is much greater than that of the shock wave propagation, so that the turbulence appears ‘frozen’ in the time scale of the wave system ($L/a_\infty \approx 0.1\text{--}0.5$ s). That is, the turbulent field does not change appreciably in the time that it takes for the entire wave system to pass a given point. This observation also suggests that the atmospheric fluctuations are not significantly modified by their interaction with the shock waves. The fluctuations appear to pass through the leading-edge shock wave relatively undisturbed, allowing them to interact in the same way with the trailing-edge shock wave.

The sixth observation may indicate that the direction in which the shock wave is propagating with respect to a given turbulent eddy or shear layer is important since a notable difference between the incident and reflected shock waves is their orientation. On the other hand, Crow (1969) argued that different distortions to the incident and reflected waves were recorded because they ‘follow widely separate paths . . . , and they intercept entirely different eddies,’ which implies that the shock wave retains some memory of past interactions, and that these effects accumulate as the wave progresses through the atmosphere.

The above observations present a complicated picture of the interaction phenomena associated with weak shock waves propagating in a heterogeneous medium. Over the past few decades some light has been shed on the relevant interaction mechanisms, but a consistent explanation for all of the observed behaviour remains elusive. Traditionally, linear model equations were sought to explain the phenomena since the situation may appear to fit within the framework of linear acoustics (Kovácsnay 1953; Ribner 1955). Unfortunately, the assumptions inherent in these linear theories are invariably violated for situations involving very weak shock waves, where propagation speeds fluctuate near the nominal free-stream speed of sound, $a_\infty = \sqrt{\gamma RT_\infty}$.

In the present paper we elaborate and extend a nonlinear theory introduced in Rusak, Giddings & Cole (1995). We provide a detailed analysis of the solution breakdown in various linear theories for general, three-dimensional, continuous acoustic waves in heterogeneous media, and not just for one-dimensional, discontinuous waves as discussed in Rusak *et al.* (1995). A close examination of this breakdown allows us to explicitly relate the scales used in the mathematical derivation of the transonic interaction theory directly to physical manifestations of the interaction – the forward scattered waves. A modified and more general derivation of the nonlinear transonic interaction equations, originally given in Rusak *et al.* (1995), is then presented. The current approach helps to emphasize the relationship between the linear and nonlinear theories. Finally, we demonstrate that all six characteristics observed in the sonic-boom data, described by Crow (1969) and listed above, can be explained by the transonic theory.

2. Breakdown of linear theories

Linear theories fail to account for the behaviour described in the preceding section, but it is enlightening to study their breakdown. For cases involving weak pressure waves propagating in weakly heterogeneous media, linear theories have historically

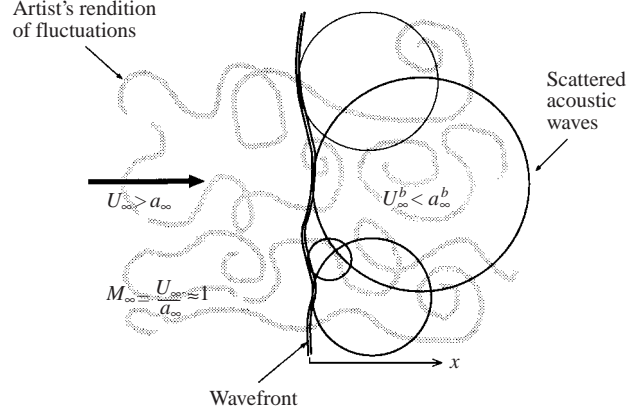


FIGURE 4. Framework for the interaction problem.

been divided into two categories (see more details in the following analysis). The breakdown of a particular linear theory can be attributed to one of two different causes depending on which category the theory falls into. While these linear theories invariably fail, their failure points the way to a richer, more successful, nonlinear theory.

The sonic-boom problem is a concrete example of a more fundamental problem: the interaction of a weak shock wave with free-stream heterogeneities. If we make the coordinate transformation to a system attached to the wavefront, as suggested in figure 1, the sonic-boom problem fits into a more basic framework with a stationary, nominally planar shock wave and a nominally uniform flow moving perpendicular to the wavefront (see figure 4). The flow has a nominal free-stream speed, U_∞ , which is nearly equal to the nominal free-stream speed of sound, a_∞ , so that the nominal free-stream Mach number is very close to one, $M_\infty = U_\infty/a_\infty \approx 1$. In reality, the free-stream flow carries with it slight fluctuations in the vorticity and the thermodynamic variables which interact with the shock wave, giving rise to scattered acoustic waves in the subsonic region behind the wavefront.

For the problem under consideration, the diffusive effects of heat conduction and viscosity may be neglected, and the Euler equations are used as the starting point:

$$\frac{\partial \rho}{\partial t} + \nabla \cdot (\rho \mathbf{u}) = 0, \quad (1)$$

$$\rho \left(\frac{\partial \mathbf{u}}{\partial t} + \mathbf{u} \cdot \nabla \mathbf{u} \right) = -\nabla p, \quad (2)$$

$$\frac{\partial p}{\partial t} + (\mathbf{u} \cdot \nabla)p + \gamma p (\nabla \cdot \mathbf{u}) = 0. \quad (3)$$

Equation (1) is the continuity equation, equation (2) is the momentum equation, and equation (3) is the energy balance equation.

It is assumed that all perturbations to the nominally uniform flow are very small. Accordingly, the following expansions for the velocity, density, and pressure may be proposed for the flow behind the shock wavefront:

$$\mathbf{u} = U_\infty^b (\hat{e}_x + \epsilon \mathbf{u}_1^c + \delta \mathbf{u}_2 + \dots), \quad (4)$$

$$\rho = \rho_\infty^b (1 + \epsilon \rho_1 + \dots), \quad (5)$$

$$p = p_\infty^b (1 + \epsilon p_1 + \dots), \quad (6)$$

where U_∞^b , ρ_∞^b , and p_∞^b are the nominal free-stream speed, density, and pressure behind the shock wavefront, respectively. To demonstrate the ideas, we concentrate only on the acoustic waves, which are confined behind the shock wavefront, and assume that the leading-order perturbation velocity vector \mathbf{u}_1^c is compressible, or irrotational (indicated by the superscript c), i.e.

$$\nabla \times \mathbf{u}_1^c = 0. \quad (7)$$

This term accounts for the leading-order acoustic field and it satisfies the radiation condition, namely that $\mathbf{u}_1^c \rightarrow \mathbf{0}$ as $x \rightarrow \pm\infty$. The $O(\delta)$ term of the velocity vector is general, i.e. $\nabla \cdot \mathbf{u}_2 \neq 0$ and $\nabla \times \mathbf{u}_2 \neq 0$.

Since the perturbations are assumed weak we specify that $\epsilon \ll 1$ and $\delta \ll 1$, but $\delta \ll \epsilon$ in the sense that $\delta/\epsilon \rightarrow 0$ in the limit as both $(\delta, \epsilon) \rightarrow 0$. This means that the vorticity waves are taken to be weaker than the compressible, or pressure, waves in this limit. If we took $\delta \sim \epsilon$, the pressure and vorticity waves would simply uncouple (see Kovásznyai 1953), and there would be no interaction between them.

We also non-dimensionalize the independent variables for position $\mathbf{x} = (x, y, z)$ and time t in the following way:

$$\bar{\mathbf{x}} = \frac{\mathbf{x}}{\ell} \quad \text{and} \quad \bar{t} = \frac{U_\infty^b t}{\ell} = \frac{t}{t_c}, \quad (8)$$

where ℓ is some generic length scale. The characteristic time, $t_c = \ell/U_\infty^b$, measures how long it takes to move a distance ℓ when traveling with speed U_∞^b . It is assumed here that the spatial scaling is uniform.

Based on these expansions we can derive two basic relations (see also Cole & Cook 1986; Landahl 1961). First, we note that for very weak disturbances all changes are nearly isentropic. More precisely,

$$\frac{p}{\rho^\gamma} = \frac{p_\infty^b}{(\rho_\infty^b)^\gamma} (1 + O(\epsilon^3)). \quad (9)$$

Substituting expansions (5) and (6), we obtain the entropy relation:

$$p_1 = \gamma \rho_1 + \epsilon \gamma \frac{\gamma - 1}{2} \rho_1^2 + \dots, \quad (10)$$

which relates the changes in our two primary thermodynamic variables.

We can derive another relationship using the momentum equation (2). Noting that \mathbf{u}_1^c can be expressed as the gradient of a velocity potential Φ , or

$$\mathbf{u}_1^c = \nabla \Phi = \frac{1}{\ell} \bar{\nabla} \Phi, \quad (11)$$

where $\bar{\nabla}$ is the gradient operator in the $(\bar{x}, \bar{y}, \bar{z})$ -coordinate system. Using (10) and (11), and substituting the expansions (4)–(6) into the momentum equation (2), we obtain the leading-order Bernoulli equation:

$$\rho_1 = -M^2 (\Phi_{\bar{t}} + \Phi_{\bar{x}}) + \dots, \quad (12)$$

where the subscripts on the scalar Φ indicate partial differentiation. $M = U_\infty^b/a_\infty^b$ is the nominal Mach number behind the wavefront. The entropy relation (10) and the Bernoulli equation (12), taken together, relate the thermodynamic variables, ρ and p , to the kinematic variable, $\mathbf{u}_1^c = \nabla \Phi$. The vorticity perturbation, contained in \mathbf{u}_2 , does not enter into the leading-order linear analysis of the acoustic waves.

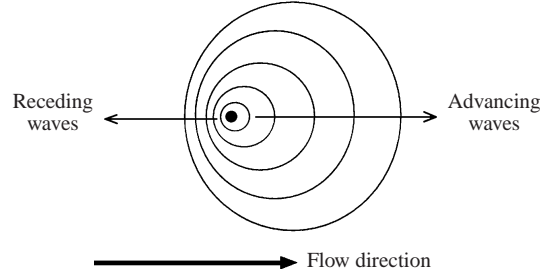


FIGURE 5. Wavefronts generated by a subsonic acoustic source.

Finally, substitution into the continuity equation yields the following linear wave equation for the velocity potential Φ :

$$(1 - M^2)\Phi_{\bar{x}\bar{x}} + \Phi_{\bar{y}\bar{y}} + \Phi_{\bar{z}\bar{z}} - M^2\Phi_{\bar{t}\bar{t}} - 2M^2\Phi_{\bar{x}\bar{t}} = 0, \quad (13)$$

where we note that $|1 - M^2| \ll 1$ for our problem, and, therefore, the first term in this equation is small. As mentioned above, we can categorize two classical linear approaches to this interaction problem based on whether or not the small term $(1 - M^2)\Phi_{\bar{x}\bar{x}}$ is retained. Both approaches are unsuccessful, but for different reasons.

When we neglect the first term in (13) we remove some of the essential physics, and the problem becomes a mathematical exercise. In this case, we find that the waves ‘pile up’ due to the superposition of the various scattered waves generated by the interaction at the wavefront, and the expansions (4)–(6) quickly become misordered. On the other hand, when we retain the first term in (13) the solution breakdown is more closely related to the physical situation; using the above assumptions, we have linearized an essentially nonlinear phenomena, and some important terms have been neglected. As a result, the predicted pressure field ‘blows up’ in the vicinity of the wavefront and the expansions become immediately misordered.

In either case, the resulting linear equation can be transformed into the canonical form of the Wave Equation,

$$\Phi_{\bar{\zeta}\bar{\zeta}} + \Phi_{\bar{\eta}\bar{\eta}} + \Phi_{\bar{\zeta}\bar{\tau}} - \Phi_{\bar{\tau}\bar{\tau}} = 0. \quad (14)$$

The solution breakdown can be examined using a fairly simple problem: a harmonically oscillating source situated in a uniform axial transonic flow, stationary in (\bar{x}, \bar{t}) -coordinates, and with intensity $\epsilon \ll 1$. We consider the subsonic case, $M < 1$, since the scattered acoustic waves are confined to the subsonic region behind the wavefront. This situation is depicted in figure 5. As the source pulsates, the waves moving against the flow, the *receding waves*, have their progress impeded and their wavefronts bunch together. The waves moving with the flow, the *advancing waves*, are propelled faster and spread out.

To see what happens when we drop the small term, $(1 - M^2)\Phi_{\bar{x}\bar{x}}$, we make a transformation to the canonical form (14),

$$\tau = \frac{1}{M}\bar{t}, \quad \bar{\zeta} = \frac{1}{M}(\bar{x} - \bar{t}), \quad \bar{\eta} = \bar{y}, \quad \bar{\zeta} = \bar{z}. \quad (15)$$

We solve the problem for Φ directly (see Appendix for details). The pressure field is obtained using equations (10) and (12).

In eliminating the small term from the linear wave equation we have removed the distinction between the wave speed and the free-stream convection speed, which are nearly, but not exactly, equal. In so doing, the receding waves travelling upstream

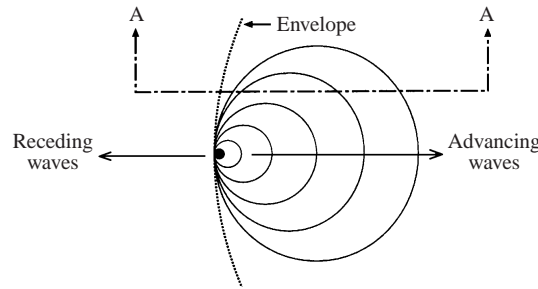


FIGURE 6. Linearized subsonic acoustic source (case 1).

coalesce, or ‘pile up’, forming an envelope that tends asymptotically in time to the $x = 0$ plane (see figure 6). The waves locally reinforce one another by superposition, and as more waves are generated the magnitude of the pressure field grows with time, so that the harmonic forcing introduces a non-harmonic, secular term in the solution.

Figure 7 shows the solution at three instants in the scaled time, \bar{t} , taken along the cut A–A indicated in figure 6. The expansions obviously become misordered. Many attempts to model the interaction phenomena have encountered this problem, including the studies by Ellison (1951), Crow (1969), George & Plotkin (1971), and Plotkin & George (1972). It is interesting to note that a similar problem arises when treating elastic waves in heterogeneous solids using a straightforward homogenization technique (see Boutin & Auriault 1993).

George & Plotkin (1971) and Plotkin & George (1972) resorted to the second-order problem in an attempt to fix the secular first-order term. But, once the expansions become misordered and the assumptions used in the perturbation procedure are violated, appeals to higher-order terms are unavailing. Also, there was some misunderstanding of the hyperbolic nature of the shock wave, which was pointed out by Ffowcs Williams & Howe (1973), and also mentioned by Pierce & Maglieri (1972) in reference to the first-order scattering theory of Crow (1969). In any event, the second-order results also suffer the same ‘pile-up’ problem and are also invalid near the wavefront.

Others have attempted to repair the linear approach by restoring the small term, $(1 - M^2)\Phi_{\bar{x}\bar{x}}$, and, in essence, have dealt with equation (13). This equation can be transformed into the canonical (14) form with the following change of variables:

$$\left. \begin{aligned} \tau &= \bar{t} + \frac{M^2}{(1 - M^2)} \bar{x}, & \xi &= \frac{M}{(1 - M^2)} \bar{x}, \\ \eta &= \frac{M}{\sqrt{1 - M^2}} \bar{y}, & \zeta &= \frac{M}{\sqrt{1 - M^2}} \bar{z}. \end{aligned} \right\} \quad (16)$$

As it turns out, this transformation is actually more important than the solutions achieved since it helps point the way to a successful model. But, before we consider the new approach, we examine what happens when we solve equation (13).

For this case, we have restored the distinction between the wave speed and the free-stream convection speed, and the receding waves are again distinct as indicated in figure 8. The pressure field scales like

$$p_1 \sim \frac{\epsilon}{1 - M^2} \quad (17)$$

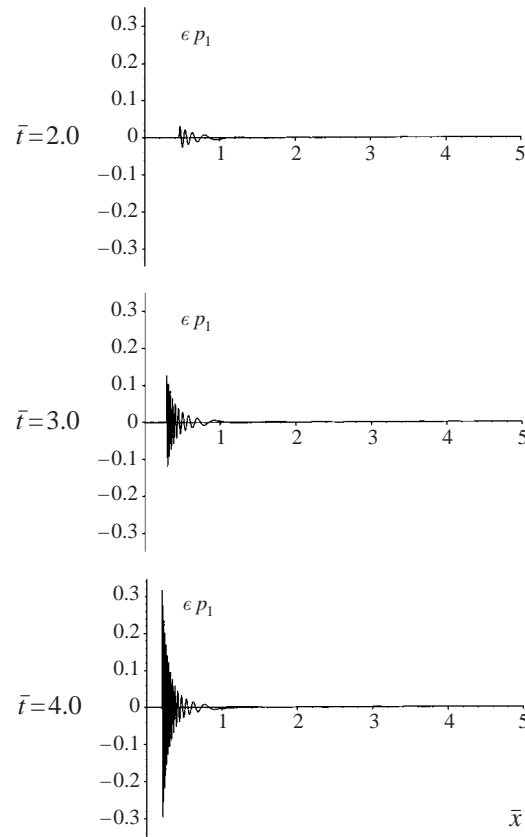


FIGURE 7. 'Pile-up' of receding waves at the envelope.

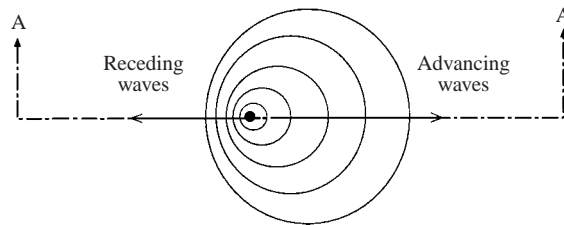


FIGURE 8. Linearized subsonic acoustic source (case 2).

and it is obvious that a problem will arise as the free-stream Mach number approaches one, $M \rightarrow 1$, with fixed ϵ (see Appendix for details).

Figure 9 shows the profile of the pressure perturbation, p_1 , for two different Mach numbers, taken along the line A–A indicated in figure 8. For a moderate Mach number $M = 0.6$ we see that the pressure perturbation is of the same order of magnitude as the source intensity (ignoring the physically meaningless singularity at the origin). The receding waves bunch up but remain distinct, and the advancing waves spread out as expected.

When we consider the solution for $M = 0.9$, which is within the transonic range, we find that the pressure perturbations of the receding waves are much stronger than the intensity of the acoustic source. As we approach Mach number one with a fixed ϵ ,

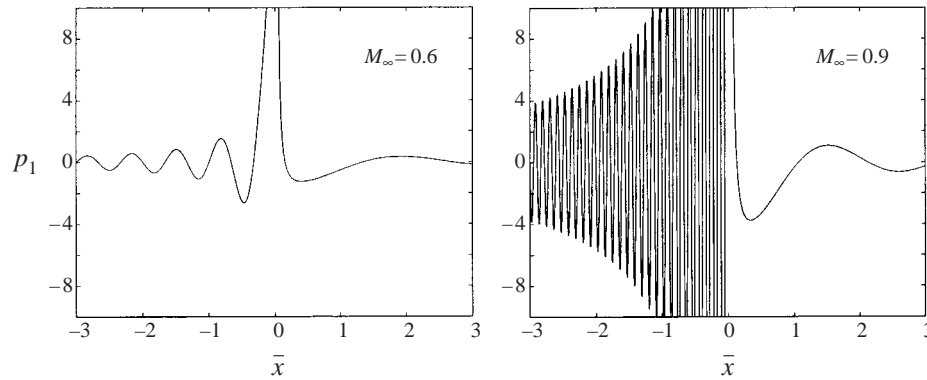


FIGURE 9. 'Blow-up' of pressure field for receding waves.

the assumption of small perturbations is violated, the pressure perturbations become huge, and this makes no physical sense. This problem was encountered by Lighthill (1953), for example.

The problem in this case is due to the fact that the flow relative to the source is moving at a nearly sonic speed, and the streamtubes are nearly incompressible in the directions transverse to the flow—the y - and z -directions. A fluid at near-sonic speeds requires a very large pressure gradient to effect a small change in the transverse streamtube area. Conversely, a very small compression (or expansion) in these directions produces a disproportionately large pressure perturbation. This behaviour is not modelled correctly by the linear theories. Flows moving transonically must be treated differently. The physics is inherently nonlinear, and this must be reflected in the mathematical model.

The linear theories produce misordered or singular solutions and necessarily fail to describe all of the interaction phenomena. In fact, the leading-order equations do not even predict an interaction, as was shown by Kováznay (1953). But, while linear theories cannot describe the interaction, they do provide much needed information concerning the various physical scales inherent in the problem. They also provide clues as to what crucial physical mechanisms must be restored in the analysis in order to achieve a uniformly valid theory. A derivation of a new theory is presented in the next section.

3. Transonic interaction theory

The derivation of the nonlinear, transonic model equation for the interaction of pressure waves with weak free-stream heterogeneities follows from different asymptotic expansions for the dependent variables, and different scalings of the independent variables. It is recognized that there are two competing small perturbations: one due to the small free-stream disturbances and the other due to the slight deviation of the nominal wave speed or the free-stream flow speed, U_∞ , from the nominal speed of sound, a_∞ . The modified spatial and temporal scalings are used to resolve the receding waves, which were responsible for the solution breakdown of the linear theories.

The strength of the shock wave and that of the free-stream fluctuations must tend uniformly to zero. To build a consistent model we must make the scaling in relation (17) explicit and take this into account when deriving our equations. To preserve the proper ordering of the terms, the ratio $\epsilon/(M_\infty^2 - 1)$ must be $O(1)$, or

$\epsilon \sim M_\infty^2 - 1$. Alternatively, we set

$$M_\infty^2 = 1 + K \epsilon \quad (18)$$

where $M_\infty > 1$ corresponds to the nominal free-stream Mach number ahead of the wavefront (as opposed to $M < 1$ in the subsonic region behind the wavefront). K is an $O(1)$ similarity parameter that relates the strength of the free-stream fluctuations to the deviation of the wave speed from the speed of sound.

To capture the critical nonlinear effects, a rescaling of the \bar{x} -coordinate and the time is also needed. The correct rescaling is suggested by the transformation (16). When transformed into the canonical form of equation (14) the waves appear to spread out isotropically in the spatial directions (ξ, η, ζ) . We use the transformation (16) to find the characteristic length in the x -direction, ℓ_x , relative to the characteristic length in the transverse y - and z -directions, ℓ , in the physical, (x, y, z) -coordinate system:

$$\frac{\ell_x}{\ell} = \frac{\partial \bar{x} / \partial \xi}{\sqrt{\partial(\bar{y}, \bar{z}) / \partial(\eta, \zeta)}} = \sqrt{M_\infty^2 - 1}, \quad (19)$$

or

$$\ell_x = \sqrt{M_\infty^2 - 1} \ell \sim \epsilon^{1/2} \ell. \quad (20)$$

This length scale, ℓ_x , corresponds to the characteristic length of the receding waves, which are ‘bunched up’ and, therefore, much shorter than the waves propagating in the transverse directions.

With this rescaling, we obtain the transonic spatial coordinates:

$$x^* = \frac{x}{\epsilon^{1/2} \ell}, \quad y^* = \frac{y}{\ell}, \quad z^* = \frac{z}{\ell}. \quad (21)$$

This rescaling stretches the x -axis and magnifies the flow field about the wavefront of the shock so that the length scale of the receding waves in the new coordinate system is of order one. It should be noted that $|1 - M_\infty^2| = M_\infty^2 - 1$ for cases involving a normal shock, where M_∞ is taken to be the supersonic Mach number, $M_\infty > 1$, ahead of the shock wave rather than the subsonic Mach number, $M < 1$, behind the wavefront, where the scattered acoustic waves reside.

To obtain a proper rescaling of the time coordinate we observe that lines of constant τ in transformation (16) are moving slowly in the negative \bar{x} -direction; they follow points on the receding waves. We can calculate the speed of these receding waves,

$$\frac{dx}{dt} = \frac{(M_\infty^2 - 1)}{M_\infty^2} U_\infty \sim \frac{\epsilon U_\infty}{M_\infty^2}. \quad (22)$$

Using this as the characteristic speed of the problem, and using the length scale for the receding waves, ℓ_x , we obtain the following rescaled time variable:

$$t^* = \frac{U_\infty \epsilon}{\ell_x M_\infty^2} t \sim \frac{U_\infty \epsilon^{1/2}}{\ell} t. \quad (23)$$

This rescaling restricts consideration to low-frequency dynamics, corresponding to the slow motion of the receding waves. With the rescaled coordinates (x^*, y^*, z^*, t^*) , we capture the dynamics of the receding waves, which dominate the flow behaviour in the vicinity of the wavefront, whereas with the linear theories discussed in the previous section we could only resolve the advancing waves.

Finally, we allow for slight variations in the vorticity. As noted in the previous section, and as demonstrated by Kovásznyai (1953), the vorticity waves do not interact

with the pressure, or acoustic, waves according to the leading-order equations of the linear theories. We can admit them in the transonic model, however. In order to include the effect of the weak vorticity perturbations, with strength δ , that interact with the shock wave, we choose the following matching condition:

$$\epsilon \iff \delta^{2/3}, \tag{24}$$

so that relatively weak perturbations to the vorticity field are coupled to the leading-order acoustic field.

This suggests the following expansions for the velocity, density, and pressure:

$$\left. \begin{aligned} \mathbf{u} &= U_\infty(\hat{e}_x + \delta^{2/3}\mathbf{u}_1 + \delta\mathbf{u}_2 + \delta^{4/3}\mathbf{u}_3 + \dots), \\ \rho &= \rho_\infty(1 + \delta^{2/3}\rho_1 + \delta^{4/3}\rho_2 + \dots), \\ p &= p_\infty(1 + \delta^{2/3}p_1 + \delta^{4/3}p_2 + \dots). \end{aligned} \right\} \tag{25}$$

The leading-order velocity perturbation $\mathbf{u}_1 = (u_1, v_1, w_1)$ contains the leading-order pressure waves which satisfy the radiation condition, while $\mathbf{u}_2 = (u_2, v_2, w_2)$ and $\mathbf{u}_3 = (u_3, v_3, w_3)$ are general. The weak shock wave and the free-stream heterogeneities are both taken to be perturbations to the nominally uniform free-stream flow, whose velocity has been aligned with the x -direction.

Substituting the expansions (25) and the expression for the Mach number (18) into the Euler equations (1)–(3), and then making the transformation to the rescaled coordinates (x^*, y^*, z^*, t^*) , we find the following relations for the leading orders of the continuity equation:

$$O(\delta^{1/3}) : \quad (u_1 + \rho_1)_{,x^*} = 0, \tag{26}$$

$$O(\delta^{2/3}) : \quad (v_{1,y^*} + w_{1,z^*}) + u_{2,x^*} = 0, \tag{27}$$

$$O(\delta) : \quad \rho_{1,t^*} + (\rho_1 u_1)_{,x^*} + (v_{2,y^*} + w_{2,z^*}) = -(\rho_2 + u_3)_{,x^*}, \tag{28}$$

where the subscripts following the comma indicate partial differentiation. The leading orders of the equation for the balance of momentum in the x -direction are given by

$$O(\delta^{1/3}) : \quad \left(\frac{1}{\gamma} p_1 + u_1 \right)_{,x^*} = 0, \tag{29}$$

$$O(\delta^{2/3}) : \quad u_{2,x^*} = 0, \tag{30}$$

$$O(\delta) : \quad u_{1,t^*} + (K + \rho_1 + u_1)u_{1,x^*} = - \left(\frac{1}{\gamma} p_2 + u_3 \right)_{,x^*}. \tag{31}$$

The leading orders of the y -momentum and z -momentum equations are given, respectively, by

$$O(\delta^{1/3}) : \quad v_{1,x^*} = 0, \tag{32}$$

$$O(\delta^{2/3}) : \quad v_{2,x^*} = -\frac{1}{\gamma} p_{1,y^*} \tag{33}$$

and

$$O(\delta^{1/3}) : \quad w_{1,x^*} = 0, \tag{34}$$

$$O(\delta^{2/3}) : \quad w_{2,x^*} = -\frac{1}{\gamma} p_{1,z^*}. \tag{35}$$

Since v_1 and w_1 must satisfy the radiation condition, equations (32) and (34) imply that $v_1 = 0$ and $w_1 = 0$.

The leading orders of the energy equation become

$$O(\delta^{1/3}) : \quad \left(\frac{1}{\gamma} p_1 + u_1 \right)_{,x^*} = 0, \quad (36)$$

$$O(\delta^{2/3}) : \quad (v_{1,y^*} + w_{1,z^*}) + u_{2,x^*} = 0, \quad (37)$$

$$O(\delta) : \quad \frac{1}{\gamma} p_{1,t^*} + \frac{u_1}{\gamma} p_{1,x^*} + p_1 u_{1,x^*} + (v_{2,y^*} + w_{2,z^*}) = - \left(\frac{1}{\gamma} p_2 + u_3 \right)_{,x^*}. \quad (38)$$

Equations (36) and (37) are redundant as they correspond to the leading orders of the x -momentum equation.

Note that equations (27) and (30) give

$$v_{1,y^*} + w_{1,z^*} = 0, \quad (39)$$

so that, in the absence of the radiation condition, the flow is incompressible to the leading order in the transverse y - and z -directions. This anticipates one of the problems encountered with the linear theories, whereby the streamtube area was incorrectly allowed to expand and contract in the transverse plane, and the pressure field blew up.

From the first-order continuity equation (26) we find that

$$u_1 + \rho_1 = f(y^*, z^*, t^*) \quad (40)$$

so that the combination $u_1 + \rho_1$ does not vary in the x -direction. Similarly, from the first-order equation for the momentum in the x -direction (29), we find that

$$u_1 + \frac{1}{\gamma} p_1 = g(y^*, z^*, t^*), \quad (41)$$

so the combination $u_1 + p_1/\gamma$ does not vary in the x -direction either. Since both of these functions, f and g , must satisfy the boundary conditions upstream, they are prescribed by the free-stream, heterogeneous field ahead of the wavefront. The function f is connected to the variations in the thermodynamic properties, while the function g is directly related to the vorticity field. There is no variation of these functions in the x -direction because the length scale of the free-stream heterogeneities is much greater than that of the receding waves and, therefore, these heterogeneities do not vary appreciably over distances comparable to the wavelength of the receding waves.

Equating the left-hand sides of equations (31) and (38), we obtain the following relation involving only the leading-order perturbations:

$$\left(u_1 - \frac{1}{\gamma} p_1 \right)_{,t^*} + (K + u_1 + \rho_1 - p_1) u_{1,x^*} - \frac{u_1}{\gamma} p_{1,x^*} - (v_{2,y^*} + w_{2,z^*}) = 0.$$

Then, using relations (40) and (41) to eliminate the thermodynamic variables, ρ_1 and p_1 , we obtain

$$2u_{1,t^*} + ((K - \gamma g + f) + (\gamma + 1)u_1) u_{1,x^*} - (v_{2,y^*} + w_{2,z^*}) = g_{,t^*}. \quad (42)$$

This gives a wave equation involving only the leading-order velocity perturbations to the uniform flow field (see also Rusak *et al.* 1995). The shock wave, free-stream fluctuations, and acoustic response to the interaction are all taken to be perturbations to the nominally uniform free-stream flow, and are described by f , g , u_1 , v_2 , and w_2 . It

is noted that, since the flow is nearly incompressible in the transverse directions, the higher-order compressibility effects in these directions result in a lower-order change in the streamwise velocity. Equations (40) and (41) relate the perturbations of the thermodynamic variables, p_1 and ρ_1 , to the velocity perturbation in the x -direction, u_1 .

Two additional relations for the velocity perturbations are needed to close the system. The equations relating the transverse vorticity fluctuations and the u_1 velocity component provide the needed constraints:

$$u_{1,y^*} - v_{2,x^*} = g_{,y^*}, \quad (43)$$

$$u_{1,z^*} - w_{2,x^*} = g_{,z^*}. \quad (44)$$

These are obtained from equations (33) and (35), and substituting for p_1 using equation (41). Together, equations (42)–(44) comprise a new system of equations for the propagation of a weak, nominally planar shock wave in a weakly heterogeneous fluid medium.

It is possible to transform equations (42)–(44) into a nonlinear, scalar equation in terms of the velocity potential, ϕ , of the pressure waves:

$$2\phi_{,x^*t^*} + ((K + g + f)\phi_{,x^*} + \frac{1}{2}(\gamma + 1)(\phi_{,x^*})^2)_{,x^*} - (\phi_{,y^*y^*} + \phi_{,z^*z^*}) = -g_{,t^*}, \quad (45)$$

since the vorticity field is prescribed completely by the function g , as we will see presently. Here we have used the substitutions

$$u_1 = \phi_{,x^*} + g, \quad v_2 = \phi_{,y^*}, \quad \text{and} \quad w_2 = \phi_{,z^*}, \quad (46)$$

which satisfy the constraints (43) and (44) identically.

While the model equation (45) is equivalent to that described in Rusak *et al.* (1995), here we have demonstrated the breakdown in the solutions of the linear models in a general three-dimensional setting and for continuous acoustic waves; in Rusak *et al.* (1995) we considered only the breakdown of the one-dimensional shock jump relations. In the present paper we have also connected the characteristic time and length scales to the receding wave field, whereas previously little justification was given for the scaling. Furthermore, in the present paper the expansions of the flow variables were arrived at systematically, and the coupling of the pressure and vorticity waves has been dealt with explicitly.

Mathematically speaking, equation (45) is an extended version of the classical transonic small-disturbance (TSD) equation which arises in transonic aerodynamics. The classical TSD equation is recovered if we set the free-stream perturbation functions, f and g , to zero. Similar equations—that is, equations with the same convective nonlinearity—were derived in connection with caustics in geometric acoustics (see Cramer 1981; Cramer & Seebass 1978; Gill & Seebass 1973; Hayes 1968; Seebass 1970). Equation (45) is also similar to the KKZ equation, which describes the propagation of nonlinear sound beams with a narrow angular spectrum in an inviscid fluid (see Gurbatov, Malakhov & Saichev 1991; Kuznetsov 1971; Zabolotskaya & Khorkhlov 1969).

As already mentioned, the functions f and g relate to the free-stream disturbances. In particular, the function g is related to the free-stream vorticity vector, $\boldsymbol{\omega} = \nabla \times \mathbf{u} = \delta^{2/3}(\omega_{x^*}, \omega_{y^*}, \omega_{z^*}) + \dots$ (where any subscripts not following a comma are just indices), namely

$$\omega_{x^*} = 0, \quad \omega_{y^*} = \frac{1}{\gamma} g_{,z^*}, \quad \omega_{z^*} = -\frac{1}{\gamma} g_{,y^*}. \quad (47)$$

Also, if we expand the entropy s variable as

$$s = s_\infty(1 + \delta^{2/3}s_1 + \dots) \quad (48)$$

we find that

$$s_1 = \frac{c_v}{S_\infty}(g - \gamma f). \quad (49)$$

The convected free-stream fluctuations—that is, the vorticity waves and the entropy waves, as opposed to the pressure waves, which propagate—are completely specified by the functions f and g . According to the present theory, the free-stream fluctuations are not affected by the weak shock wave or the scattered pressure waves, although the converse is not true. A similar result was also described in the numerical simulations of Lee *et al.* (1993).

We can examine the shock jump conditions, which illuminate some of the observed behaviour mentioned in the Introduction. If the shock surface is given by

$$\bar{x} = \epsilon^{1/2}h(\bar{y}, \bar{z}, \epsilon^{-1/2}\bar{t}) \quad \text{or} \quad x^* - h(y^*, z^*, t^*) = 0 \quad (50)$$

we obtain the following shock jump relations:

$$-2[u_1] h_{,t^*} + (K + g + f)[u_1] + (\gamma + 1)[u_1]\langle u_1 \rangle + [v_2] h_{,y^*} + [w_2] h_{,z^*} = 0 \quad (51)$$

and

$$[f] = 0, \quad [g] = 0, \quad (52)$$

$$[v_2] + [u_1] h_{,y^*} = 0, \quad (53)$$

$$[w_2] + [u_1] h_{,z^*} = 0, \quad (54)$$

where the jump in φ is $[\varphi] = \varphi_b - \varphi_a$, the average of φ , $\langle \varphi \rangle = (\varphi_b + \varphi_a)/2$, and the subscripts a and b indicate the values immediately ahead of and behind the wavefront, respectively.

Equation (52) indicates that there is no jump in either f or g across the wavefront, so the interaction with the shock wave does not modify the convected, free-stream fluctuations. The convected heterogeneities distort the shock wave and produce scattered pressure waves, but there is no reciprocal effect, and so the free-stream fluctuations pass through the shock wave unchanged to the leading order. This may explain the observation of Crow (1969) (characteristic 5 in the Introduction) that the leading-edge and trailing-edge shock waves experience the same distortion pattern, since they interact with the same, unmodified heterogeneities, which appear frozen in the time scale of the sonic-boom wave system.

Also, since the vorticity and the thermodynamic gradients are vector fields, the orientation of the shock wave dictates the nature of the interaction. For example, in the special case where the vorticity vector and the normal to the shock surface are colinear the theory predicts no distortion at all to the shock wave; but, if the wavefront were oriented in any other way relative to the vorticity there would be a distortion. This may explain the observation of Crow (1969) (characteristic 6 in the Introduction) that incident and reflected waves experience different distortions when they encounter the same vorticity pattern. Referring to figure 10, we observe that the incident and reflected waves make different angles with the local vorticity, so according to the present theory the interactions should produce different effects. The same holds for free-stream thermodynamic gradients.

In the next section we examine the nature of the interaction with some relatively simple numerical simulations. The traditional, stochastic approach is premature, and clouds the issue concerning the appropriate mathematical modelling of the relevant physical mechanisms. In the light of this, we treat various deterministic problems with

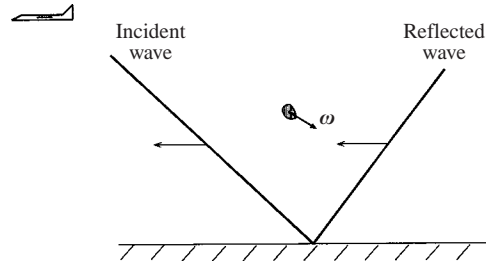


FIGURE 10. Orientation of incident and reflected wavefronts with respect to a patch of vorticity.

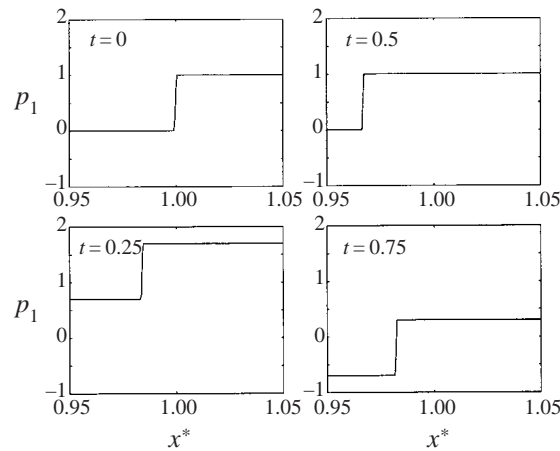


FIGURE 11. Motion of planar shock wave subject to a variable mean wind (the plot for $t = 1.0$ is the same as that for $t = 0$).

specific free-stream fluctuation patterns through the specification of the functions f and g . The numerical examples provide more insight into the observations of Crow (1969) listed in the Introduction.

4. Numerical results

For all of the calculations presented here the numerical scheme of Engquist & Osher (1980), which is a modification to the Murman & Cole (1971) method, is used. Periodic boundary conditions in the transverse directions and a non-reflecting outflow boundary condition were used, and the shock wave was generated by placing a normal shock in a uniform flow. At the inflow boundary, $\phi_{y^*y^*} = g_{t^*}$ was specified to reflect that the variations in the free-stream perturbations in the stretched x^* -coordinate are exceedingly small. Mesh-refinement convergence studies were conducted on all simulations (see Giddings 1999), and only the fully converged results are shown.

To make the conversions between the characteristic scales in the physical and transonic coordinate systems we refer to table 1. Here L is the characteristic length scale in the physical coordinates, measured in feet or metres; and, L^* is the corresponding, dimensionless length scale in the transonic coordinates, which is given by the relation (21). The associated time scales follow from (23). The characteristic, physical time scale is denoted by T and measured in seconds; the dimensionless, transonic time is denoted by T^* .

Scales	L (ft, m)	L^*	T (s)	T^*
L	—	$\frac{\sqrt{M_\infty^2 - 1}}{K} \ell L^*$	$U_\infty T$	$\frac{K M_\infty^2}{\sqrt{M_\infty^2 - 1}} \ell T^*$
L^*	$\frac{K}{\sqrt{M_\infty^2 - 1}} \frac{L}{\ell}$	—	$\frac{1}{\sqrt{M_\infty^2 - 1}} \frac{U_\infty T}{\ell}$	$\frac{(K M_\infty)^2}{M_\infty^2 - 1} T^*$
T	$\frac{L}{U_\infty}$	$\sqrt{M_\infty^2 - 1} \frac{\ell L^*}{U_\infty}$	—	$\frac{M_\infty^2}{\sqrt{M_\infty^2 - 1}} \frac{\ell T^*}{U_\infty}$
T^*	$\frac{\sqrt{M_\infty^2 - 1}}{K M_\infty^2} \frac{L}{\ell}$	$\frac{M_\infty^2 - 1}{(K M_\infty)^2} L^*$	$\frac{\sqrt{M_\infty^2 - 1}}{M_\infty^2} \frac{U_\infty T}{\ell}$	—

TABLE 1. Conversion chart for characteristic scales.

The similarity parameter K is set to $K = (\gamma + 1)/2\gamma = 0.857$ for all cases computed so that the nominal jump in p_1 across the planar shock wave is $\Delta p_1 = 1.0$. When we consider a nominal pressure jump across the shock wave of 1 lb ft^{-2} , which is typical for sonic-boom measurements, this corresponds to an upstream Mach number of about $M_\infty \approx 1.0002$. In the Introduction, we observed that the mean free-stream fluctuations had very little, if any, effect on the magnitude and character of the shock wave (see Crow 1969, characteristic 1 in the Introduction). To demonstrate this, we examine the effect of a variable mean wind with the new model equations by specifying

$$g = \cos(2\pi t^*). \quad (55)$$

This corresponds to a slight, unsteady, and spatially uniform fluctuation in the uniform flow speed. Figure 11 shows how the shock wave adjusts to this particular type of disturbance by accelerating and decelerating, so that the speed of the flow remains constant relative to the shock wave. The strength of the shock is unchanged as the wavefront simply adjusts its speed in order to maintain its fixed strength. It is important to note that the sonic-boom shock wave, at great distances from the aircraft that generated it, is free to move, unlike a shock attached to a physical boundary, which is constrained.

We next consider a nominally planar shock wave and a steady, sinusoidal pattern of vorticity convected through it, with

$$g = \cos(2\pi y^*). \quad (56)$$

This would correspond physically to a slight, sinusoidal wind shear, where the velocity gradient is in only one direction. Here, we only consider the gradients in the transverse y -direction. The results are shown in figure 12, and two things are immediately apparent. First, the wave has been amplified locally (at $y^* = 0, 1$) to almost twice the nominal strength, as shown in figure 13(a). Relative amplifications of this magnitude are commonly observed in sonic-boom pressure measurements (see Garrick 1968; Garrick & Maglieri 1968; Hubbard *et al.* 1964; Kane 1967; Kane & Palmer 1964). This result is consistent with the observation of Crow (1969) (characteristic 3 in the Introduction).

Also, at $y^* = 0.5$ there is a smooth compression, which makes it appear as though the shock has been diffused, or ‘thickened’, as shown in figure 13(b). The pattern of

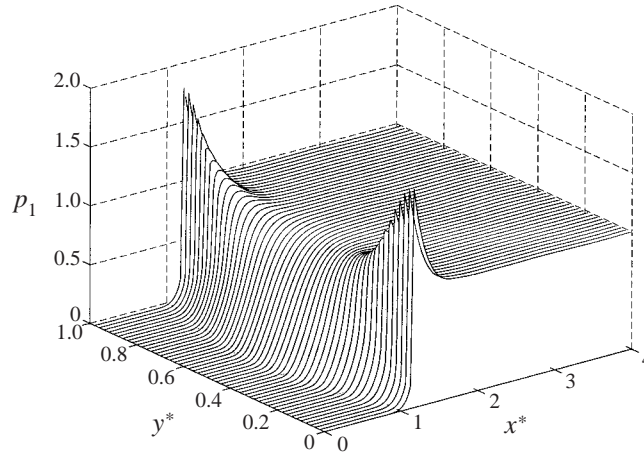


FIGURE 12. Distortion of shock wave due to a sinusoidal pattern of vorticity.

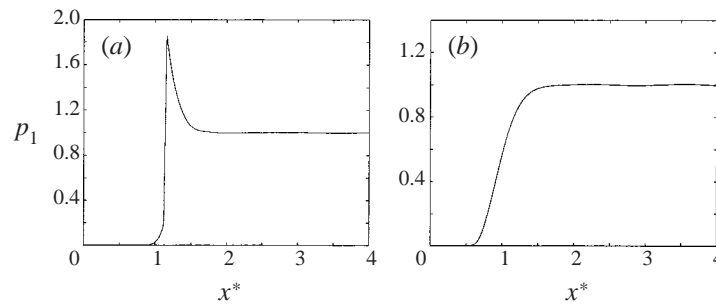


FIGURE 13. Shock wave at various positions along the wavefront: (a) peaked, $y^* = 0.1$; (b) rounded, $y^* = 0.5$.

vorticity given by equation (56) produces a pocket of slightly subsonic air relative to the shock wavefront. When the shock wave encounters this pocket, the shock decays locally to zero strength and, therefore, allows a smooth transition through the sonic point. The decay of the shock into a smooth compression around $y^* = 0.5$ is contained in the TSD model equations (42)–(44); it is not attributable to physical diffusion nor is it a numerical artifact. This result is consistent with the observation of Crow (1969) (characteristic 2 in the Introduction).

There is also evidence to suggest that the thickening of the shock may be caused, at least in part, by the relaxation of the vibrational energy modes of the molecules, which are excited when the fluid molecules pass through the shock wave (see Reed 1977; Bass *et al.* 1983, 1987). Estimates based on these models account for considerable thickening, but they still underpredict the degree of thickening that has been measured experimentally for the sonic-boom problem. It should also be pointed out that the shock thickness increases as the strength of the shock wave decreases, and for very weak shocks the thickness can be several orders of magnitude larger than the mean free path (see Thompson 1988, § 7.10, for example).

It is important to note that the theory presented herein only predicts a smooth compression (without a jump discontinuity) when the magnitude of the fluctuation, $|g|$, is greater than the similarity parameter K . In figure 14 we see what occurs when the free-stream fluctuations are relatively strong compared to the shock strength

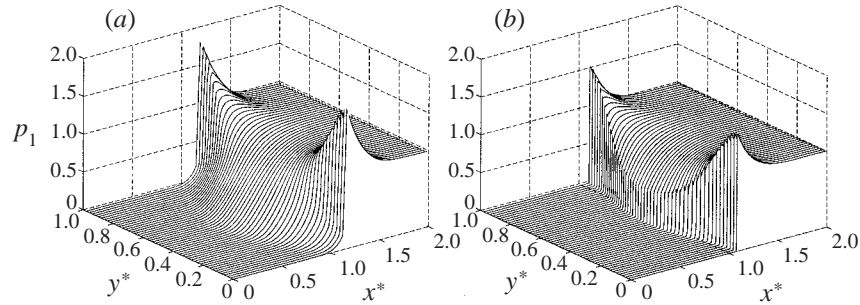


FIGURE 14. Comparison of the distorted shock wave for free-stream fluctuations where: (a) $|g| = 1.0$, $K = 0.857$ ($|g| > K$); and, (b) $|g| = 0.5$, $K = 0.857$ ($|g| < K$).

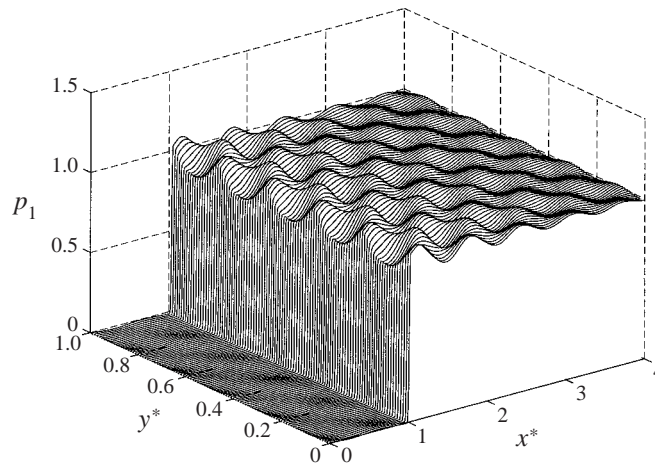


FIGURE 15. Interaction of weak shock wave with small-scale, isotropic fluctuations ($t^* = 2.0$).

($|g| > K$), and also when the fluctuations are relatively weak ($|g| < K$). In the former case, figure 14(a), the free-stream fluctuations are strong enough to smear out the shock wave and remove the discontinuous jump in the middle of the wavefront. In the latter case, figure 14(b), the shock wavefront is distorted but remains discontinuous, and there is a pressure rise due to defocusing behind the weakened portion of the wavefront ($y^* \approx 0.5$), where the streamtube area increases, the fluid speed decreases, and the pressure increases.

We also consider another example with an isotropic free-stream disturbance pattern. This is a simplified model for isotropic 'turbulence', where the length scales of the coherent turbulent structures, or 'eddies', are the same in all directions. We consider an example where the eddies have a characteristic length of $L = 1/5$ ft, where $\ell = 1$ ft. The characteristic time scale of the free-stream fluctuations in the transonic coordinates is $T^* \approx 0.00466$. The free-stream disturbance pattern is given by

$$g = \cos(10\pi y^*) \cos(10\pi t^*/0.00466). \quad (57)$$

Referring to figure 15, we find that the shock is not significantly amplified or thickened, but there are small-scale pressure waves behind the shock wave. These waves constitute the diffraction pattern of the receding waves, which were generated

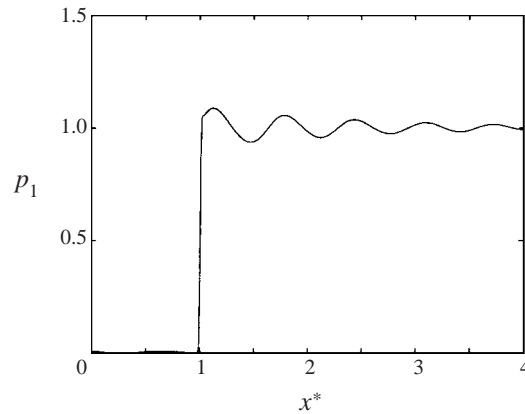


FIGURE 16. Pressure profile due to isotropic fluctuations.

by the interaction at the wavefront and confined to the subsonic region behind the shock.

Figure 16 shows a typical pressure profile across the shock wave. The pressure waves behind the wavefront have a length scale of $L^* \approx 0.5$, which is equivalent to a physical scale of about $L = 1.17 \times 10^{-2}$ ft, or 3.56×10^{-3} m. This demonstrates how the length scales of the pressure spikes are much smaller than the fluctuations which gave rise to them (by a factor on the order of $\sqrt{1 - M_\infty^2}$). Also, the amplitude of the pressure spikes decays rapidly behind the wavefront, which is due to the fact that the stronger receding waves are confined to the region immediately behind the wavefront, and also due to geometrical attenuation as the obliquely scattered waves spread out (cylindrically in this example) from their source. The attenuation rate would be even greater in three dimensions due to the enhanced geometric attenuation of spherical acoustic waves. This result is consistent with another observation of Crow (1969) (characteristic 4 in the Introduction).

Finally, we combine the effects of 'wind shear' and 'turbulence' by specifying

$$g = 0.5 \cos(2\pi y^*) + (\cos(10\pi y^*) \cos(10\pi t^*/0.00466)). \quad (58)$$

Referring to figure 17, we find that the shock wavefront has been significantly distorted, and there are also small-scale pressure waves behind the wavefront. In fact, many of the qualitative features of the sonic-boom pressure profiles observed by Crow (1969) are manifested in the resulting pressure field (characteristics 2–4 in the Introduction).

In figure 18 we show the pressure profiles across the shock wave at various stations for a given time. In figure 18(a) we observe an amplified shock wave with small-scale pressure spikes behind, which resembles the peaked profile depicted in the Introduction, only stretched. Again, the length scales of the spikes are about $L = 1.17 \times 10^{-2}$ ft, or 3.56×10^{-3} m. Figure 18(b) shows a smooth, or rounded, profile where the shock appears to be thickened. Qualitatively, both results in figure 18(a,b) agree with the experimental observations mentioned in the Introduction (see Garrick 1968; Garrick & Maglieri 1968; Hubbard *et al.* 1964; Kane 1967; Kane & Palmer 1964).

The amplified shock shown in figure 18(a) is almost twice as strong as the nominal shock wave, which is what we would expect from actual measurements of weak shock interactions with strong turbulence. Also, the increase in shock thickness shown in

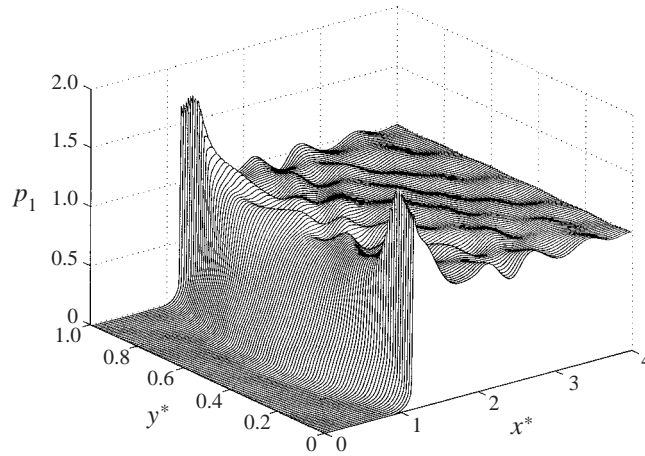


FIGURE 17. Interaction with isotropic and anisotropic vorticity fields ($t^* = 2.0$).

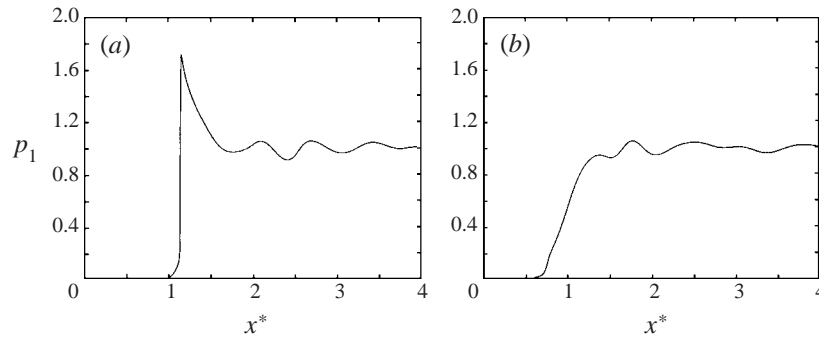


FIGURE 18. Pressure profiles across various positions along the wavefront: (a) peaked, (b) rounded.

figure 18(b) is about $\Delta x^* \approx 0.4$. This corresponds to a thickness in physical coordinates of about $\Delta x \approx 9.34 \times 10^{-3}$ ft, or about 2.85×10^{-3} m, which is several orders of magnitude greater than the nominal shock thickness ($\sim 1 \times 10^{-6}$ m). Again, this result is not due to the diffusive mechanisms of viscosity and heat conduction, nor to a lack of numerical resolution or convergence; rather, it is due to the local, nonlinear interaction of the shock wave with strong turbulent fluctuations, which allows a smooth compression. This degree of shock thickening is also in line with experimental recordings of sonic-boom pressure profiles (listed in the previous paragraph).

5. Conclusions and discussion

The interaction of weak shock waves and slight heterogeneities in the media can be studied using asymptotic methods. We first demonstrated the breakdown of the solutions according to the linear theories, and described two possible solution breakdown mechanisms. In both cases, the breakdown occurred in the solution of the receding wave field. This suggested a special rescaling of the spatial and temporal coordinates that resolves the receding waves. It was also observed that the interaction problem involves two competing small perturbations: the $O(M_\infty^2 - 1)$ shock wave strength, and $O(\delta)$ the strength of the free-stream heterogeneities. By stipulating that

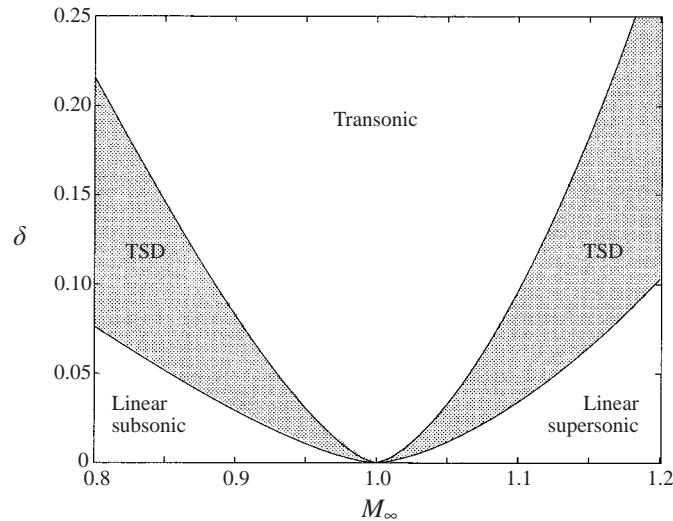


FIGURE 19. Range of applicability for the transonic theory.

these two small perturbations tend uniformly to zero and rescaling the independent variables, we obtain a nonlinear model which describes the interaction phenomena.

Numerical simulations of shock waves interacting with simple free-stream fluctuations display all six of the essential features observed in sonic-boom measurements (Crow 1969), which were enumerated in the Introduction. The theory attributes the observed amplification and the shock thickening to anisotropic shear winds, gusts, and thermal gradients with variations in the directions transverse to the wavefront. Also, as observed, the theory shows that small-scale isotropic fluctuations do not have a measurable effect on the shock thickness and they produce relatively minor amplification to the shock wave. These small-scale waves did, however, produce the smaller-scale pressure spikes behind the wavefront, which correspond to the interference pattern of the various, scattered receding waves.

Another result of the present theory is that the leading-order interaction effects are confined to the acoustic waves, whereas the vorticity and entropy waves remain unchanged by the interaction. This would allow successive wavefronts, arriving from the same direction, to interact with the same (unmodified) heterogeneity, and experience the same distortion. Furthermore, it was shown that the orientation of the vorticity with respect to the acoustic wavefront has a strong influence on the nature of the interaction, which would explain the observed characteristic that the wavefronts arriving from different directions experience different interaction effects when they pass the same point in a heterogeneous medium.

Unlike linear theories, the transonic model equations predict behaviour at the wavefront which is physically meaningful and consistent with experimental observations. It is important to understand the range of applicability of the theory, however. If we take the magnitude of the free-stream disturbances to be $O(\delta)$, and the nominal free-stream Mach number relative to the shock wave is M_∞ , then figure 19, which follows from relations (18) and (24), gives a rough idea as to when the theory is valid. If the free-stream disturbance strength $O(\delta)$ scales with M_∞ as shown in the shaded region of figure 19, then the TSD theory is applicable, so long as the free-stream Mach number, M_∞ , is fairly close to one. It should be emphasized that for the specific case

where M_∞ is extremely close to one, a direct numerical simulation of the interaction is very complicated and has never been done before.

For free-stream Mach numbers around $M_\infty \approx 1.05$, where the Mach number behind the shock wavefront is $M \approx 0.95$, the nonlinear effects are expected to be less pronounced. Here $(1 - M^2)^{-1} \approx 10$ and the pressure field as described by equation (13) does not produce solutions that are grossly misordered, which is borne out by the scaling indicated in equation (17). The nonlinear effects are also confined to the shock wavefront region. The direct numerical simulations of Lee *et al.* (1993), which demonstrated good agreement with the Linear Interaction Analysis of Ribner (1954, 1955, 1969, 1987), included computations in this regime, and significant nonlinear effects were noted. It should also be noted that Lee *et al.* (1993) mainly considered situations where $K \gtrsim 2$, which is significantly larger than the values considered here, and this would also lead one to expect weaker nonlinearities.

If the free-stream disturbances are much weaker than the shock wave strength, which varies like $M_\infty^2 - 1$, then the similarity parameter K becomes large and the transonic equation is essentially reduced to a linear equation which does not predict a strong interaction to the leading order. On the other hand, when the free-stream disturbances are relatively strong we fall in the transonic region, which may require a richer nonlinear theory than the one presented here. Also, as the shock wave becomes stronger, and M_∞ becomes considerably larger than one, the results are no longer valid (despite the fact that the expansions may remain well-ordered) because the assumptions that underlie the theory no longer hold. Most notably, the flow processes are no longer isentropic to the leading orders.

This work was supported by the NASA Langley Research Center under grant number NAG-1-1362, and by the Office of Naval Research under grant number N00014-97-1-0687.

Appendix

Here we present the solution of the two linear equations where a source at the origin, $(\bar{x}, \bar{y}, \bar{z}) = (0, 0, 0)$, with intensity $\exp(2\pi k i \bar{t}) H(\bar{t})$ has been specified, where $H(\cdot)$ is the Heaviside function. First we consider the case where the small term, $(1 - M^2)\Phi_{\bar{x}\bar{x}}$, has been dropped from equation (13). The resulting equation is

$$\Phi_{\bar{y}\bar{y}} + \Phi_{\bar{z}\bar{z}} - M^2\Phi_{\bar{t}\bar{t}} - 2M^2\Phi_{\bar{x}\bar{t}} = 0. \quad (\text{A } 1)$$

In this case no distinction is made between the convection speed and the free-stream speed of sound. The solution for the potential Φ is

$$\Phi_I = -\frac{M}{\bar{x}} \exp\left(-i\pi k \frac{2\bar{x}\bar{t} - \bar{x}^2 - M^2(\bar{y}^2 + \bar{z}^2)}{M\bar{x}}\right) H\left(\frac{2\bar{x}\bar{t} - \bar{x}^2 - M^2(\bar{y}^2 + \bar{z}^2)}{2M\bar{x}}\right). \quad (\text{A } 2)$$

The pressure perturbation is given by

$$p_1 = -\gamma M^2(\Phi_{\bar{t}} + \Phi_{\bar{x}}), \quad (\text{A } 3)$$

which is found using equations (10) and (12). It is obvious that the pressure field contains a secular term, growing linearly with time \bar{t} , arising from the $(2\bar{x}\bar{t})$ cross-term in the exponent. That is, the pressure field due to a harmonic source is non-harmonic. This is displayed in figure 7. The waves are seen to 'pile up', and the acoustic field grows in strength causing the expansions to become misordered.

Figure	ϵ	M	k	\bar{t}	\bar{y}	\bar{z}
7	0.0001	0.9	5.0	2, 3, 4	1.0	1.0
9	NA	0.6, 0.9	1.0	1.0	0.0	0.0

TABLE 2. Conversion chart for characteristic scales.

For the second case we restore the small term, $(1 - M^2)\Phi_{\bar{x}\bar{x}}$, and solve equation (13),

$$(1 - M^2)\Phi_{\bar{x}\bar{x}} + \Phi_{\bar{y}\bar{y}} + \Phi_{\bar{z}\bar{z}} - M^2\Phi_{\bar{t}\bar{t}} - 2M^2\Phi_{\bar{x}\bar{t}} = 0. \tag{A 4}$$

For this case the distinction between the convection speed and the free-stream speed of sound is restored. The solution for the potential Φ is

$$\Phi_{II} = \frac{\exp\left(2\pi ki\left(\bar{t} + \frac{M^2}{(1 - M^2)}\bar{x} \pm \frac{M\sqrt{\bar{x}^2 + (1 - M^2)(\bar{y}^2 + \bar{z}^2)}}{(1 - M^2)}\right)\right)}{\sqrt{\bar{x}^2 + (1 - M^2)(\bar{y}^2 + \bar{z}^2)}}, \tag{A 5}$$

where we have dropped the Heaviside function, since Φ_{II} and its derivatives are harmonic. The pressure perturbation, given by equation (A 3), is

$$\epsilon p_1 = \frac{\gamma M^2 k}{2|\bar{x}|} \left(\frac{1}{1 - M}\right) \sin\left(2\pi k\left(\bar{t} + \frac{1}{1 - M}\bar{x}\right)\right) - \frac{\gamma M^2 k}{4\pi\bar{x}^2} \cos\left(2\pi k\left(\bar{t} + \frac{1}{1 - M}\bar{x}\right)\right) \tag{A 6}$$

for the receding waves along the x -axis ($\bar{y} = \bar{z} = 0$). Equation (A 6) is valid for $\bar{x} < 0$, and we note that the first term on the right-hand side is responsible for the ‘blow up’. The effect is physically related to the sonic throat problem of quasi-one-dimensional flows in converging–diverging nozzles, where the fluid is nearly incompressible in the transverse directions.

For the advancing waves we have

$$\epsilon p_1 = \frac{\gamma M^2 k}{|\bar{x}|} \left(\frac{1 + 2M}{1 + M}\right) \sin\left(2\pi k\left(\bar{t} + \frac{1}{1 - M}\bar{x}\right)\right) - \frac{\gamma M^2}{4\pi\bar{x}^2} \cos\left(2\pi k\left(\bar{t} + \frac{1}{1 - M}\bar{x}\right)\right) \tag{A 7}$$

Equation (A 7) is valid for $x > 0$, and it is well-ordered – that is, $O(1)$.

Table 2 provides the parameters and coordinates used to generate the graphs in figures 7 and 9. The independent variables are in the shock-attached coordinate system given by equation (8).

REFERENCES

BASS, H. E., EZELL, J. & RASPET, R. 1983 Effect of vibrational relaxation on rise times of shock waves in the atmosphere. *J. Acoust. Soc. Am.* **74**, 1514–1517.
 BASS, H. E., LAYTON, B. A., BOLEN, L. N. & RASPET, R. 1987 Propagation of medium strength shock waves through the atmosphere. *J. Acoust. Soc. Am.* **82**, 306–310.
 BOUTIN, C. & AURAUULT, J. L. 1993 Rayleigh scattering in elastic composite materials. *Intl J. Engng Sci.* **31**, 1669–1689.
 COLE, J. D. & COOK, L. P. 1986 *Transonic Aerodynamics*. North-Holland.
 CRAMER, M. S. 1981 The focusing of weak shock waves at an axisymmetric arête. *J. Fluid Mech.* **110**, 249–253.

- CRAMER, M. S. & SEEBASS, A. R. 1978 Focusing of weak shock waves at an arête. *J. Fluid Mech.* **88**, 209–222.
- CROW, S. C. 1969 Distortion of sonic bangs by atmospheric turbulence. *J. Fluid Mech.* **37**, 529–563.
- ELL SON, T. H. 1951 The propagation of sound waves through a medium with very small random variations in refractive index. *J. Atmos. Terrest. Phys.* **2**, 14–21.
- ENGQUST, B. & OSHER, S. 1980 Stable and entropy satisfying approximations for transonic flow calculations. *Maths Comput.* **34**, 45–75.
- FFOWCS WILLIAMS, J. E. & HOWE, M. S. 1973 On the possibility of turbulent thickening of weak shock waves. *J. Fluid Mech.* **58**, 461–480.
- GARRICK, E. I. 1968 Atmospheric effects on the sonic boom. In *Second Conf. on Sonic Boom Research, NASA SP-180* (ed. I. R. Schwartz), pp. 3–17.
- GARRICK, E. I. & MAGLER, D. J. 1968 A summary of results on sonic boom pressure signature variations associated with atmospheric conditions. *NASA TN D-4588*.
- GEORGE, A. R. & PLOTKIN, K. J. 1971 Propagation of sonic booms and other weak nonlinear waves through turbulence. *Phys. Fluids* **14**, 548–554.
- GIDDINGS, T. E. 1999 Theoretical and numerical study of the propagation of weak shock waves in weakly heterogeneous fluid media. PhD thesis, Rensselaer Polytechnic Institute.
- GILL, P. M. & SEEBASS, A. R. 1973 Nonlinear acoustic behavior at a caustic: an approximate analytical solution. *AIAA Paper 73-1037*.
- GURBATOV, S. N., MALAKHOV, A. N. & SAICHEV, A. I. 1991 *Nonlinear Random Waves and Turbulence in Nondispersive Media: Waves, Rays, Particles*, pp. 14–20. Manchester University Press.
- HAYES, W. D. 1968 Similarity rules for the nonlinear acoustic propagation through a caustic. In *Second Conf. on Sonic Boom Research, NASA SP-180* (ed. I. R. Schwartz), pp. 165–171.
- HODGSON, J. P. & JOHANNESSEN, N. H. 1971 Real-gas effects in very weak shock waves in the atmosphere and the structure of sonic bangs. *J. Fluid Mech.* **50**, 17–20.
- HUBBARD, M. H., MAGLER, D. J., HUCKEL, V. & HILTON, D. A. 1964 Ground measurements of sonic boom pressures for the altitude range of 10,000 to 75,000 feet. *NASA TR R-198*.
- KANE, E. J. 1967 Some effects of the atmosphere on sonic boom. In *Sonic Boom Research, NASA SP-147* (ed. A. R. Seebass), pp. 49–63.
- KANE, E. J. & PALMER, T. Y. 1964 Meteorological aspects of the sonic boom. *Boeing SRDS Rep. RD 64-160*.
- KOVÁSZNAY, L. S. G. 1953 Turbulence in supersonic flow. *J. Aeronaut. Sci.* **20**, 657–682.
- KUZNETSOV, V. O. 1971 Equations of nonlinear acoustics. *Sov. Phys.-Acoust.* (transl. from *Akusticheskii Z.*) **16**, 467–470.
- LANDAHL, M. T. 1961 *Unsteady Transonic Flow*. Pergamon.
- LEE, S., LELE, S. K. & MOON, P. 1993 Direct numerical simulation of isotropic turbulence interacting with a weak shock wave. *J. Fluid Mech.* **251**, 533–562.
- LIGHTHILL, M. J. 1953 On the energy scattered from the interaction of turbulence with sound or shock waves. *Proc. Camb. Phil. Soc.* **49**, 531–551.
- MURMAN, E. M. & COLE, J. D. 1971 Calculation of plane steady transonic flows. *AIAA J.* **9**, 114–121.
- PERCE, A. D. 1970 Some attempts to theorize about the anomalous rise times of sonic booms. In *Third Conf. on Sonic Boom Research, NASA SP-255* (ed. I. R. Schwartz), pp. 147–160.
- PERCE, A. D. 1971 Statistical theory of atmospheric turbulence effects on sonic-boom rise times. *J. Acoust. Soc. Am.* **49**, 906–924.
- PERCE, A. D. & MAGLER, D. J. 1972 Effects of atmospheric irregularities on sonic-boom propagation. *J. Acoust. Soc. Am.* **51**, 702–721.
- PLOTKIN, K. J. 1989 Review of sonic boom theory. *AIAA Paper 89-1105*.
- PLOTKIN, K. J. & GEORGE, A. R. 1972 Propagation of weak shock waves through turbulence. *J. Fluid Mech.* **54**, 449–467.
- REED, J. W. 1977 Atmospheric attenuation of explosion waves. *J. Acoust. Soc. Am.* **61**, 39–47.
- REBNER, H. S. 1954 Convection of a pattern of vorticity through a shock wave. *NACA Rep.* 1164 (supersedes *NACA TN 2864*).
- REBNER, H. S. 1955 Shock-turbulence interaction and the generation of noise. *NACA Rep.* 1233 (supersedes *NACA TN 3255*).
- REBNER, H. S. 1969 Acoustic energy flux from shock-turbulence interaction. *J. Fluid Mech.* **35**, 299–310.

- R BNER, H. S. 1987 Spectra of noise and amplified turbulence emanating from shock-turbulence interaction. *AIAA J.* **25**, 436–442.
- RUSAK, Z., G DD NGS, T. E. & COLE, J. D. 1995 Interaction of a weak shock with freestream disturbances. *AIAA J.* **33**, 977–984.
- SEEBASS, R. 1970 Nonlinear acoustic behavior at a caustic. In *Third Conf. on Sonic Boom Research*, NASA SP-255 (ed. I. R. Schwartz), pp. 87–120.
- THOMPSON, P. A. 1988 *Compressible-Fluid Dynamics*. Maple Press Co.
- WH THAM, G. B. 1952 The flow pattern of a supersonic projectile. *Commun. Pure Appl. Maths* **5**, 301–348.
- WH THAM, G. B. 1956 On the propagation of weak shock waves. *J. Fluid Mech.* **1**, 290–318.
- ZABOLOTSKAYA, E. A. & KHORKHLOV, R. V. 1969 Quasi-plane waves in the nonlinear acoustics of confined beams. *Sov. Phys.-Acoust.* (transl. from *Akusticheskii Z.*) **15**, 35–40.